Materials Advances

ROYAL SOCIETY OF CHEMISTRY

PAPER

View Article Online
View Journal | View Issue

Check for updates

Cite this: *Mater. Adv.*, 2023, 4, 3344

Received 27th January 2023,
Accepted 29th June 2023

DOI: 10.1039/d3ma00048f

rsc.li/materials-advances

Optimized charge transport in *N*-substituted isatin-based acceptor–donor–acceptor small molecules by regulating the side chain length for solution-processable organic thin-film transistors†

Wenyu Cai,‡[ac] Jiyun Lee,‡[b] Yao Zhao,[a] Boseok Kang *[b] and Guobing Zhang *[ac]

Side chains are necessary components of solution-processable semiconductors and exert a significant influence on charge transport. In this work, a series of acceptor–donor–acceptor (A–D–A) small molecules (**C1–C10**) based on indacenodithieno[3,2-*b*]thiophene (IDTT) as the donor and *N*-substituted isatin with different side-chains (from methyl to *n*-decyl) as acceptors were designed and synthesized for solution-processable organic thin-film transistors. The side chain length had an obvious influence on the field-effect mobility with a nearly odd–even effect. The small molecule with the methyl side chain did not exhibit any field-effect performance, while the other small molecules with longer alkyl chains showed excellent device performance with field-effect mobilities of over 1 cm^2 V^{-1} s^{-1}. In particular, the small molecules with ethyl and hexyl side-chains exhibited the highest mobilities of ~6 cm^2 V^{-1} s^{-1}. These results indicate that the minor structural modification of the side chain in A–D–A small molecules significantly affects the structural order and resulting device performance.

Introduction

Solution processable organic semiconductors have received tremendous attention in organic thin-film transistors (OTFTs) because of their high potential application in low-cost fabrication of organic electronics, such as flexible displays, chemical sensors, and smart cards.[1–3] In the past few years, significant improvements in OTFTs have been made and the field-effect performances of organic semiconductors, such as the field-effect mobilities, are larger than that of amorphous silicon due to the remarkable enhancements in molecular design and device optimization.[4,5] The molecular structures which generally contain conjugated backbones and flexible side chain structures strongly affect the molecular packings, orientation, morphology, and the corresponding charge carrier mobilities.[6]

The backbone for high-performance semiconductors features a highly planar and rigid conjugated structure which can weaken the structural disorders and enhance ordered aggregation with close molecular-packing.[7–9] For example, Michinobu *et al.* reported high-performance benzothiadiazole-naphthalenediimide-based conjugated polymers which exhibited a unipolar electron mobility of up to 7.16 cm^2 V^{-1} s^{-1} by optimizing the coplanar backbone of conformation through the introduction of intramolecular interactions (CH···O).[10]

The side chains are necessary components of all the solution-processable organic semiconductors and endow the semiconductors with excellent solubility in organic solvents. Recent research has indicated that subtle structure modification on the side chains can exert a significant effect on the structural order and charge transport properties.[11–13] For example, siloxane-terminated side chains were designed and introduced into the isoindigo-based donor–acceptor (D–A) conjugated polymers. And the π–π stacking distance (3.58 Å) of the spin-coated films was much closer compared to that of the 2-octyldodecyl side chain-based conjugated polymer with the same backbone (3.75 Å) owing to moving the position of the branching point away from the isoindigo backbone. Consequently, the corresponding OTFT devices exhibited a field-effect mobility as high as 2.48 cm^2 V^{-1} s^{-1}.[14] Side chain optimization, such as *via* modifying the type, length, and position of the branching point, is the most effective molecular engineering strategy for constructing high-performance

---

[a] Special Display and Imaging Technology Innovation Center of Anhui Province, National Engineering Lab of Special Display Technology, Academy of Opto-Electronic Technology, Anhui Province Key Laboratory of Measuring Theory and Precision Instrument, Hefei University of Technology, Hefei 230009, China. E-mail: gbzhang@hfut.edu.cn

[b] SKKU Advanced Institute of Nanotechnology, Department of Nano Science and Technology, and Department of Nano Engineering, Sungkyunkwan University (SKKU), Suwon 16419, the Republic of Korea. E-mail: bskang88@skku.edu

[c] School of Chemistry and Chemical Engineering, Key Laboratory of Advance Functional Materials and Devices of Anhui Province, China

† Electronic supplementary information (ESI) available: Experimental section (synthesis and characterization), TG, device performances, and output curves of small molecules. See DOI: https://doi.org/10.1039/d3ma00048f

‡ These authors contributed equally to this work.

OTFTs.[9,15,16] Therefore, side chains are as important as the conjugated backbone when synthesizing organic semiconductors for high-performance organic electronic devices. Despite the intensive research studies on side-chain engineering in D–A conjugated polymers, very few reports have focused on the side chain effects (such as the crystal structure, morphology, and field-effect performances) for D–A small molecules. It should be noted that the D–A small molecules have well defined structures with no batch variation and good solubility with excellent film-forming properties,[17–20] all of which make the D–A small molecules a potential candidate for high-performance semiconductors in OTFTs. Therefore, it is of great significance to investigate the effect of side chains on the molecular packing and field-effect performances of D–A small molecules.

A high performance A–D–A small molecule based on indacenodithieno[3,2-*b*]thiophene (**IDTT**) and *N*-substituted indole-2,3-dione (**IDD-N**) with a hexyl side chain was reported in our previous work.[21,22] The aza-substitution in its backbone endowed the small molecule with excellent backbone planarity, ordered crystal structures, and encouraging hole mobilities (>7 cm^2 V^{-1} s^{-1}). How the side chain affect the properties of A–D–A small molecules, an obvious next step, should be further investigated. Herein, a series of A–D–A small molecules (**IDTT-IDD-N-Cn**, abbr: **Cn**) with different side chains (from methyl to *n*-decyl) on **IDD-N** were synthesized and characterized (Scheme 1). The variation of side chains exerted a significant effect on the optical properties, microstructures, and field-effect mobilities of OTFTs. The A–D–A small molecules with even side chains (**C2**, **C4**, **C6**, **C8**, and **C10**) exhibited excellent field-effect performances with the highest mobilities of over 6 cm^2 V^{-1} s^{-1}, whereas the semiconductors with odd side chains (**C1**, **C3**, **C5**, **C7**, and **C9**) showed relatively low field-effect mobilities, especially for **C1**-based small molecules, which did not exhibit any field-effect performance due to the inferior crystal structure and morphology. These results indicated that minor structural modification of the side chain exerted a significant influence on the structural order and field-effect performances of A–D–A small molecules.

Results and discussion

Synthesis and characterization

The synthetic routes of **IDD-N** units with different side chains and small molecules are shown in Scheme 1. Ten A–D–A small molecules with the same backbone were synthesized *via* the Stille coupling reaction. **IDD-N** units with different side chains (from methyl to *n*-decyl) were added during the Stille reaction to produce the corresponding A–D–A small molecules, which were named according to the side chain length (abbr: **C1**, **C2**, **C3**, **C4**, *etc.*), respectively. The detailed synthesis is provided in the Experimental section (ESI). The structures of all the A–D–A small molecules were confirmed by nuclear magnetic resonance (NMR) spectroscopy (^{1}H NMR and ^{13}C NMR) and elemental analysis (EA). Thermogravimetric analysis (TGA) was performed to investigate the thermal stability (Fig. S1, ESI†) and the corresponding results indicated excellent thermal stabilities for all the A–D–A small molecules with decomposition temperatures (5 wt% loss temperature) of over 400 °C. Differential scanning calorimetry (DSC) results indicated that small molecules with short side chains (**C1–C3**) did not exhibit transition in the range of our study. Exothermic transitions were observed for other small molecules with longer side chains (**C4–C10**). Moreover, the transition temperatures decreased with increasing side chain length (Fig. S1, ESI†).

Optical properties and energy levels

The normalized absorption spectra of all the A–D–A small molecules in dilute chloroform solution and solid thin films are shown in Fig. 1. The corresponding data, such as absorption maximum and optical band gap, are also summarized in Table 1. First, all the small molecules in chloroform solution exhibited two same absorption bands with the maximal absorption peak of about 588–591 nm (Fig. 1a). Second, compared to the absorption in solutions, absorptions in all the films except that of **C1** showed redshifts of about 8–11 nm (Fig. 1b). For example, **C2** exhibited the maximal absorption of about 590 nm in solution, which was redshifted to 598 nm in the solid film (Table 1). These results indicated that the structural order may be improved in the solid films for **C2–C10** due to the enhanced intermolecular interactions. Moreover, the weak shoulder peaks located at about 560 nm can be also observed for the films of **C2–C10**, indicating the improvement of interchain aggregation. It should be noted that the absorption peaks of **C1** films both with and without annealing did not show any redshift compared to that of the solution, indicating that the methyl side chain in the **IDD-N** unit might be a drag on the

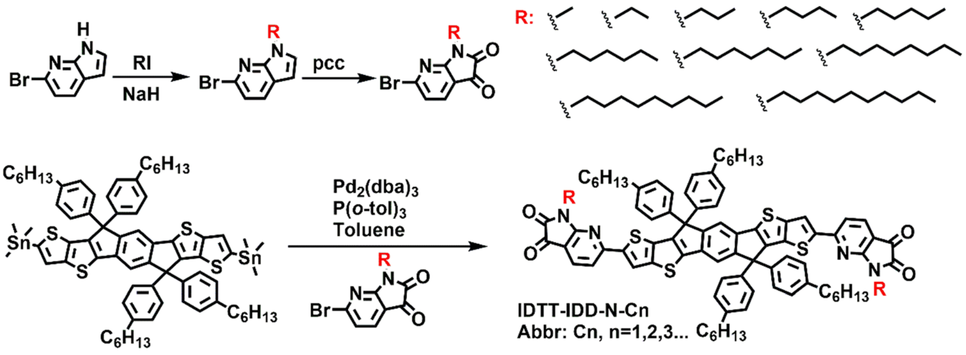

Scheme 1 Synthetic routes for monomers and small molecules.

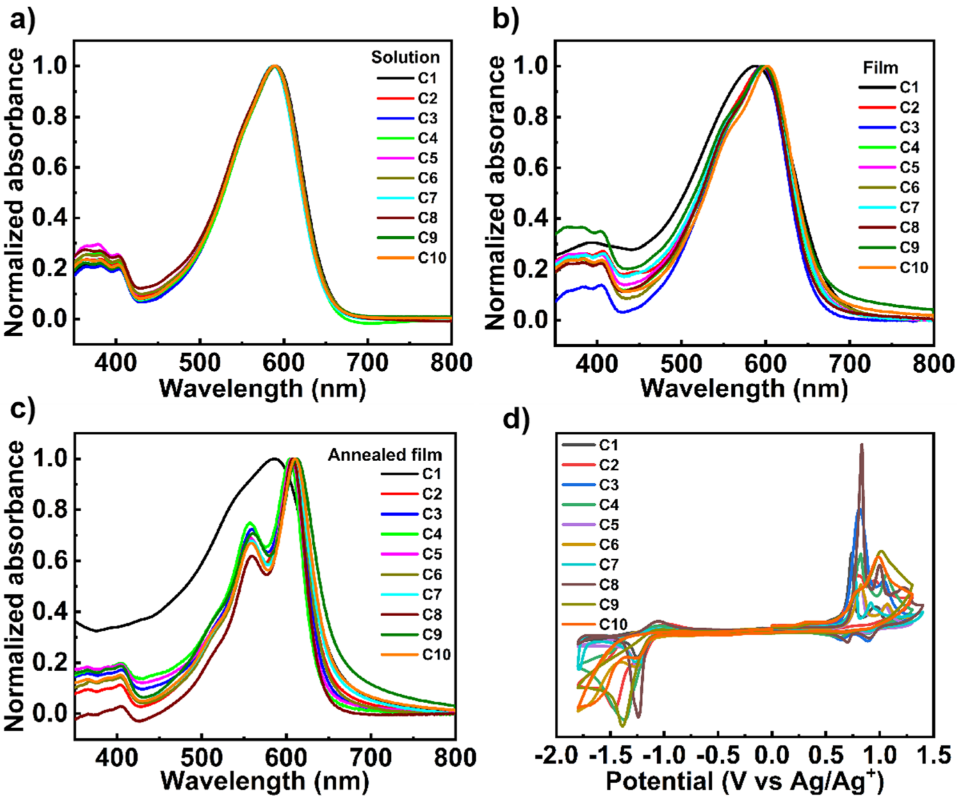

Fig. 1 (a)–(c) Normalized UV-vis spectra in chloroform solution, spin-coated thin-films from chloroform solution, and annealed films. (d) Cyclic voltammograms of small molecules.

Table 1 The thermal properties, optical properties, and energy levels of small molecules

Molecule	T_d [a] [°C]	λ_{max} [nm] Solution	Film	Annealed film	E_g^{opt} [b] [eV]	E_{HOMO} [c] [eV]	E_{LUMO} [c] [eV]	E_g^{cv} [eV]
C1	446	591	589	587	1.81	−5.40	−3.64	1.76
C2	448	590	598	607	1.82	−5.39	−3.65	1.74
C3	435	590	598	607	1.83	−5.39	−3.66	1.73
C4	455	590	598	605	1.82	−5.42	−3.65	1.77
C5	448	590	598	607	1.82	−5.42	−3.64	1.78
C6	432	590	598	608	1.81	−5.43	−3.68	1.75
C7	442	589	599	609	1.82	−5.40	−3.65	1.75
C8	456	588	597	607	1.82	−5.42	−3.64	1.78
C9	427	589	599	612	1.82	−5.40	−3.63	1.77
C10	415	590	601	610	1.82	−5.43	−3.64	1.79

[a] The 5 wt% loss temperature. [b] $E_g^{opt} = 1240/\lambda_{onset}$. [c] HOMO = $-(4.75 + E_{onset}^{ox})$ and LUMO = $-(4.75 + E_{onset}^{red})$. The redox Fc/Fc$^+$ was located at 0.05 V related Ag/Ag$^+$.

intermolecular aggregation. Finally, the annealing strategy further led to the larger redshift (7–13 nm) of maximal absorption and much stronger shoulder peaks for **C2–C10** (Fig. 1c). The results showed the further enhanced aggregation for the annealed films, which was beneficial to obtain higher performance OTFTs when the annealed films were used as the semiconductor layers. The optical band gaps were almost same for all the A–D–A small molecules with the values of about 1.81–1.83 eV (Table 1), which are calculated from absorption onset of non-annealed films.

The lowest unoccupied molecular orbital (LUMO) and the highest occupied molecular orbital (HOMO) energy levels were investigated by cyclic voltammetry (CV) characterization (Fig. 1d). The corresponding LUMO/HOMO energy levels calculated from CVs are summarized in Table 1. All the A–D–A small molecules exhibited similar LUMO (from −3.64 to −3.68 eV) and HOMO (from −5.39 to −5.43 eV) energy levels. This indicated that the different side chains in acceptors did not significantly affect the energy structure probably because of the same backbones for all the A–D–A small molecules.

Table 2 The optimized performances of small molecules based OTFT devices

Molecule	Annealing temperature (°C)	$\mu_{h,max}$ (cm^2 V^{-1} s^{-1})	$\mu_{h,avg}$ (cm^2 V^{-1} s^{-1})	V_{th} (V)	I_{on}/I_{off}
C1[a]	—	—	—	—	—
C2	210	5.93	4.13	−28.0	2.14×10^6
C3	210	3.33	3.18	−18.1	3.54×10^6
C4	240	3.51	3.27	−22.2	4.46×10^6
C5	260	1.52	1.32	−17.4	2.65×10^6
C6	210	6.29	4.69	−28.3	3.80×10^6
C7	210	1.04	0.91	−8.24	5.15×10^6
C8	210	3.25	2.61	−23.6	4.02×10^6
C9	210	1.09	0.83	−10.5	1.43×10^5
C10	210	1.69	1.28	−8.6	2.71×10^5

[a] **C1** did not exhibit any field-effect performance.

The field-effect performance of solution-processed OTFTs

To investigate the field-effect performances of the A–D–A small molecules with different side chain lengths, the OTFT devices were fabricated with the bottom-gate/top-contact (BG/TC) configurations. All the OTFT devices were characterized under ambient conditions directly. All the non-annealed (N/A) devices did not exhibit any field-effect performances. This should be ascribed to the inferior morphology which was confirmed by atomic force microscopy (AFM) characterization (Fig. S5–S12, ESI†). Similar results were also reported for other A–D–A small molecules.[21,22] It should be noted that no field-effect performances were obtained for all the **C1**-based devices even though the films were annealed at different temperatures. The results indicated that the methyl side chain in the small molecule backbone resulted in detrimental effects on the crystal structure, morphology, and charge transport. In comparison, the annealed devices based on **C2–C10** exhibited typical hole transport characteristics and the optimized device data are listed in Table 2. The field-effect mobilities fluctuated with varying the annealing temperature. The optimized temperatures were 210 °C for **C2**, **C3**, and **C6–C10**, 240 °C for **C4**, and 260 °C for **C5**, respectively. As shown in Fig. 2, the field-effect mobilities of all small molecules did not change linearly with extending side chain length (**C2–C10**). However, the fluctuation of mobility exhibited a nearly odd–even effect within the whole small molecules. The representative transfer, output curves, and fluctuation trend with side chain length are shown in Fig. 2 and Fig. S2, S3 (ESI†). **C1**, **C3**, **C5**, **C7**, and **C9** with odd-numbered side-chains exhibited the optimized hole mobilities of 0, 3.33, 1.52, 1.04, and 1.09 cm^2 V^{-1} s^{-1}, respectively. By contrast, **C2**, **C4**, **C6**, **C8** and **C10** with even-numbered side chains showed obviously higher hole mobilities of 5.93, 3.51, 6.29, 3.25 and 1.69 cm^2 V^{-1} s^{-1}, respectively. These results implied that a minor structural modification of the side chains in A–D–A small molecules led to a significant influence on the field-effect performances. For example, no field-effect performance was observed for the methyl side chain-based small molecules, while the excellent device performances with the

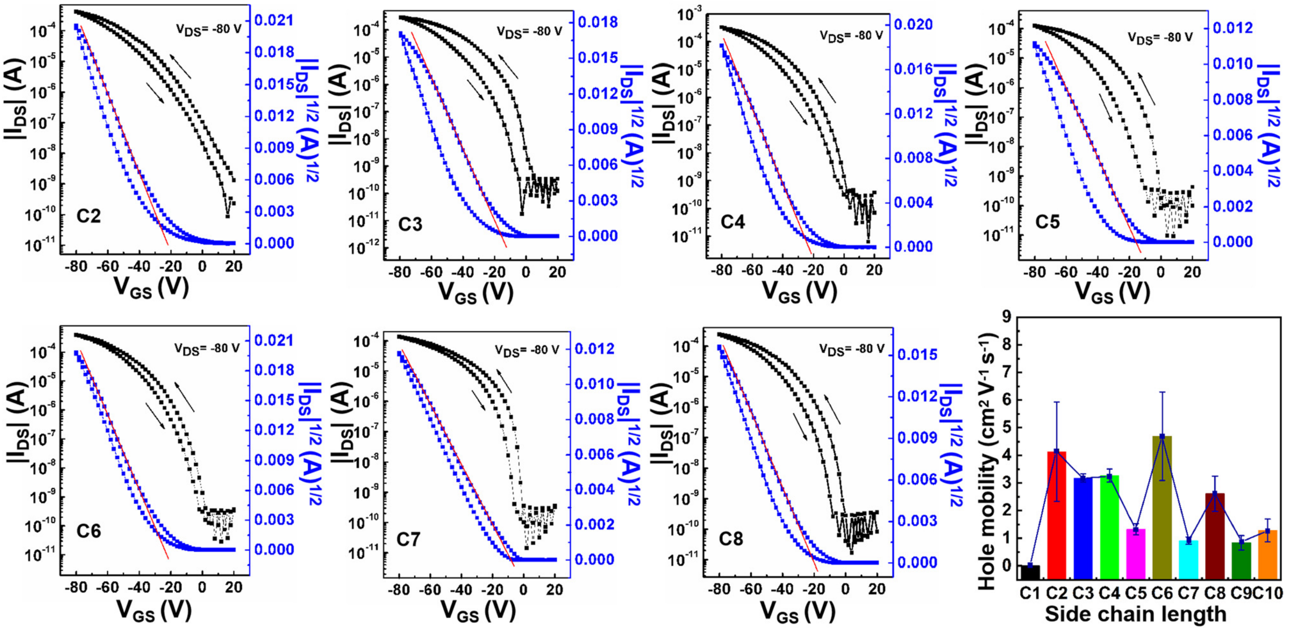

Fig. 2 Typical transfer curves of small molecules and the effect of side chain length on the field-effect mobility.

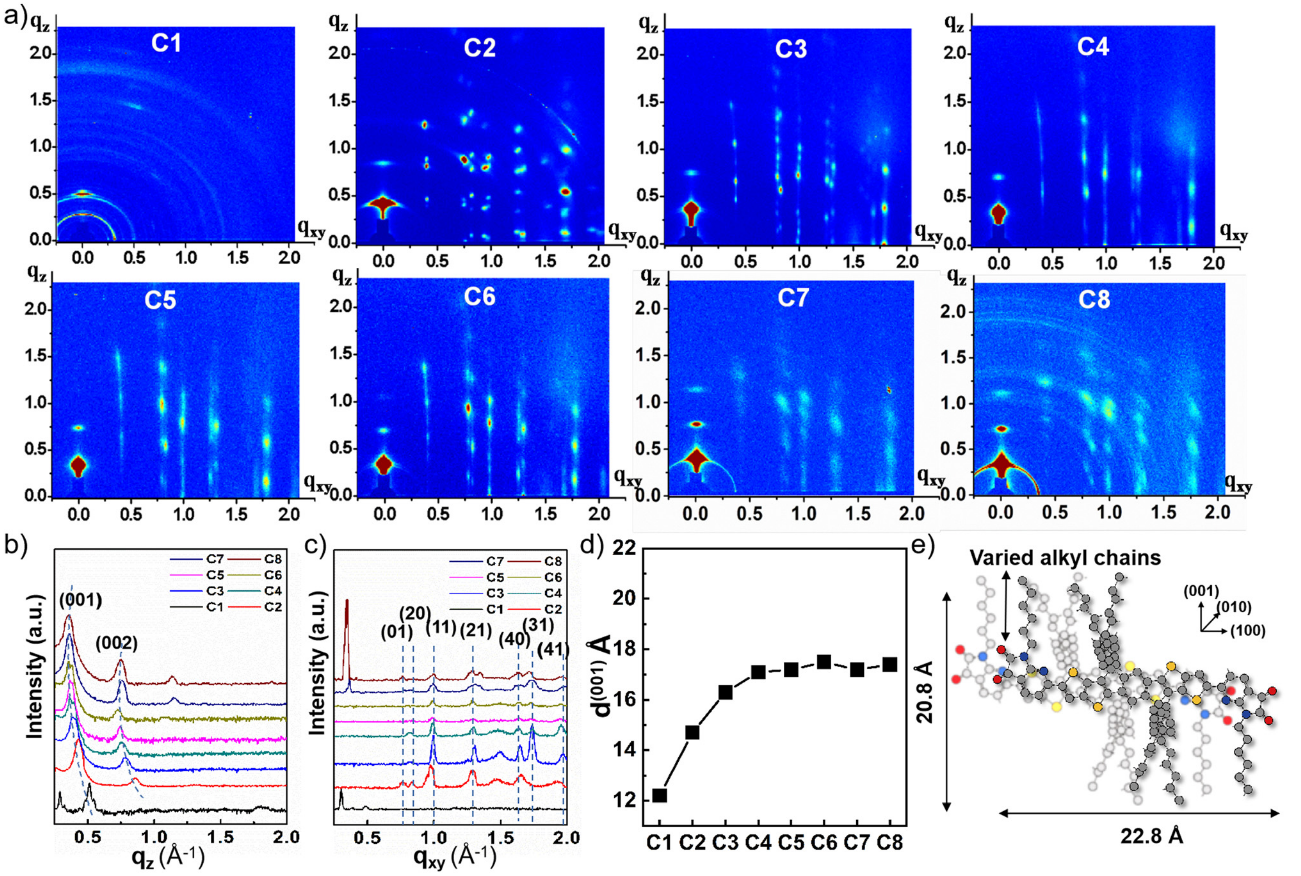

Fig. 3 (a) 2D-GIXD patterns of **C1–C8** thin films. (b) Out-of-plane and (c) in-plane X-ray intensity profiles of **C1–C8** thin films. (d) d-spacing lengths along the (001) crystalline direction as a function of alkyl chain length. The values are evaluated from 2D-GIXD patterns. (e) DFT-calculated lengths of **C6** along the long-molecular axis direction and the alkyl chain direction, where the hexyl groups attached at benzene rings are extended for simplicity of calculations.

highest mobility of ∼ 6 cm^2 V^{-1} s^{-1} were obtained for ethyl side chain-based small molecules. The distinct difference resulting from the side chain should be related to the molecular packing and structural order.

The microstructural characterization

In order to understand the changes of carrier mobilities of A–D–A small molecules with different alkyl chain lengths, the microstructures and thin film morphologies were investigated by X-ray diffraction (XRD), two-dimensional grazing incidence X-ray diffraction (2D-GIXD), and atomic force microscopy (AFM). The samples were prepared under the same conditions as the OTFT devices. The XRD patterns of films with and without annealing are shown in Fig. S4 (ESI†). The non-annealed films of all small molecules exhibited amorphous structures. In comparison, the annealed films showed obvious diffraction peaks, which were consistent with the out-of-plane GIXD. Fig. 3a shows the representative 2D-GIXD patterns of the spin-coated thin films. Except for **C1**, other small molecules showed well-ordered lamellar crystalline structures along the out-of-plane direction and several intense Bragg rods, indicating the molecules are ordered well along both vertical and horizontal directions in the film. **C1** exhibited ring patterns without a preferred molecular orientation with respect to the substrate. The disorder in the crystalline structure was well matched with the poor charge transporting properties of **C1**. By contrast, the other molecules showed a mainly standing-up configuration, where the alkyl chains are perpendicular to the substrates.

By using the 1D X-ray intensity profiles of the 2D-GIXD patterns (Fig. 3b and c), we assigned the index of each peak and estimated the d-spacings. The positions of Bragg rods were similar for the **Cn**s (n = 2–8), indicating that a- and b-axis d-spacings (*i.e.*, 15.10 Å and 7.89 Å) were nearly identical regardless of the alkyl chain lengths at the IDDN group; the estimated π–π stacking distances are half of the b-axis distance, approximately 3.9 Å. Noticeably, the (001) peaks are gradually shifted toward smaller q values as the alkyl chains are lengthened, corresponding to increased c-axis d-spacings (from 12.2 Å to 17.6 Å; Fig. 3d). A weak even–odd effect was observed in the c-axis d-spacings for some **Cn**s (n = 5–8), indicating that the number of carbons in the alkyl chain considerably affects the molecular assembly and the crystalline structure. Given the fact that the **Cn** molecule has lengths of approximately 22.8 Å and 20.8 Å along the molecular long axis and the alkyl chain direction (verified from the DFT simulated structure, Fig. 3e),

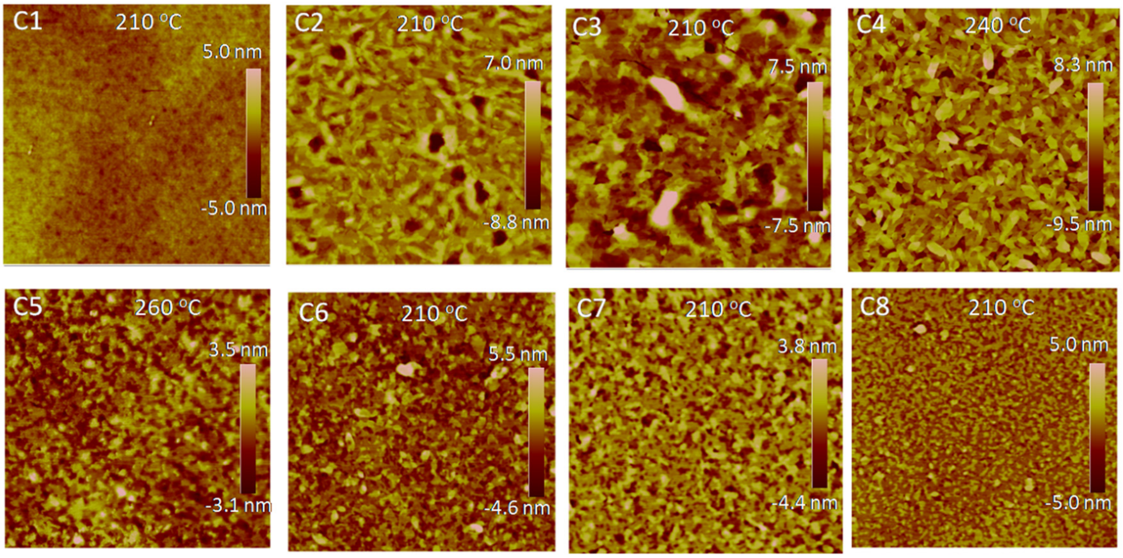

Fig. 4 The AFM height images (5 × 5 μm) of small molecules annealed at optimized temperature.

there should be interdigitation of the alkyl chains along the lamellar packing direction and a slight overlap along the molecular long axis as well, and the change of alkyl chain lengths at **IDD-N** group seems to modulate those overlap distances slightly. We propose the solid-state structure of **Cn** based on 2D–GIXD and DFT calculation (Fig. 3e). Additionally, the peak at q = 0.29 Å^{-1} in the 2D–GIXD pattern of **C1** corresponds to the *d*-spacing of 21.7 Å, which is similar to the molecular long axis distance. This result again explains the poor electrical properties of **C1**. However, to understand the significant difference in the properties of small molecules with methyl and other side chains, the single crystals may be the ideal way for providing a direct insight into the molecular arrangement. We tried our best and were also seeking help from professional organizations. Unfortunately, the single crystal was not successfully obtained probably due to the bulky aromatic side chains.

Fig. 4 shows the height AFM images of the thin films annealed at the optimized temperature, and the other AFM images annealed at different temperatures are also found in the ESI† (Fig. S5–S12). All the films without annealing exhibited very smooth surface with an amorphous nature, which can well explain the poor field-effect performances for the N/A devices. Interestingly, after annealing at different temperatures, the morphology of **C1** did not exhibit an obvious improvement, and the film still showed the smooth surface with no aggregation (Fig. S5, ESI†). The results indicated that the annealing strategy was unfavorable for the structural order of the **C1** film, which was consistent with the UV-vis results mentioned above and also well explained why the **C1**-annealing devices still showed poor OTFT performances. In comparison, the morphologies were significantly improved for the other small molecules (**C2–C8**) when the films were annealed at above 150 °C (Fig. S6–S12, ESI†). The obviously aggregated domains were formed in the whole area (Fig. 4), which should be responsible for the enhanced field-effect performances of the annealed devices.

Conclusions

Ten A–D–A small molecules based on fused-rings as the donor and *N*-substituted isatin with different side chains as acceptors were successfully synthesized for solution-processable OTFT applications. Because of the variation in the side chain, small molecules exhibited different optical characteristics, crystal structures, morphologies, and device performances. No field-effect performance was observed for **C1** with the methyl side chain, while the other small molecules exhibited excellent device performances. The fluctuation of the field-effect mobilities showed a nearly odd–even effect with varying the side chain length and the optimized mobilities of ~ 6 cm^2 V^{-1} s^{-1} were obtained for ethyl and hexyl-based small molecules.

Conflicts of interest

The authors declare no competing financial interest.

Acknowledgements

This work was supported by the National Natural Science Foundation of China (Grant No. 22175050) and the University Synergy Innovation Program of Anhui Province (GXXT-2019-001). This research was also supported by the National Research Foundation of Korea (NRF) grants (2022K1A4A7A04094482 and 2023R1A2C1005015) funded by the Ministry of Science and ICT, Korea. The authors also thank the 3C and 9A beamlines (the Pohang Accelerator Laboratory in Korea) for providing the beam time.

References

1 Y. Pan and G. Yu, *Chem. Mater.*, 2021, **33**, 2229–2257.

2 W. Zhang, Y. Liu and G. Yu, *Adv. Mater.*, 2014, **26**, 6898–6904.

3 Z. Liu, G. Zhang and D. Zhang, *Acc. Chem. Res.*, 2018, **51**, 1422–1432.

4 I. Kang, H. J. Yun, D. S. Chung, S. K. Kwon and Y. H. Kim, *J. Am. Chem. Soc.*, 2013, **135**, 14896–14899.

5 H. Sirringhaus, *Adv. Mater.*, 2014, **26**, 1319–1335.

6 Z. Zhao, Z. Yin, H. Chen, L. Zheng, C. Zhu, L. Zhang, S. Tan, H. Wang, Y. Guo, Q. Tang and Y. Liu, *Adv. Mater.*, 2017, **29**, 1602410.

7 A. F. Paterson, S. Singh, K. J. Fallon, T. Hodsden, Y. Han, B. C. Schroeder, H. Bronstein, M. Heeney, I. McCulloch and T. D. Anthopoulos, *Adv. Mater.*, 2018, **30**, 1801079.

8 Y. Liu, F. Wang, J. Chen, X. Wang, H. Lu, L. Qiu and G. Zhang, *Macromolecules*, 2018, **51**, 370–378.

9 F. Wang, Y. Dai, W. Wang, H. Lu, L. Qiu, Y. Ding and G. Zhang, *Chem. Mater.*, 2018, **30**, 5451–5459.

10 Y. Wang, T. Hasegawa, H. Matsumoto and T. Michinobu, *J. Am. Chem. Soc.*, 2019, **141**, 3566–3575.

11 J.-H. Dou, Y.-Q. Zheng, T. Lei, S.-D. Zhang, Z. Wang, W.-B. Zhang, J.-Y. Wang and J. Pei, *Adv. Funct. Mater.*, 2014, **24**, 6270–6278.

12 O. B. Berryman, V. S. Bryantsev, D. P. Stay, D. W. Johnson and B. P. Hay, *J. Am. Chem. Soc.*, 2007, **129**, 48–58.

13 T. Lei, J. H. Dou and J. Pei, *Adv. Mater.*, 2012, **24**, 6457–6461.

14 J. Mei, D. H. Kim, A. L. Ayzner, M. F. Toney and Z. Bao, *J. Am. Chem. Soc.*, 2011, **133**, 20130–20133.

15 J. Mei and Z. Bao, *Chem. Mater.*, 2013, **26**, 604–615.

16 J. Lee, A. R. Han, H. Yu, T. J. Shin, C. Yang and J. H. Oh, *J. Am. Chem. Soc.*, 2013, **135**, 9540–9547.

17 J. Wang and X. Zhan, *Acc. Chem. Res.*, 2021, **54**, 132–143.

18 Q. Zhou, Y. Jiang, T. Du, Z. Wang, Z. Liang, Y. Han, Y. Deng, H. Tian and Y. Geng, *J. Mater. Chem. C*, 2019, **7**, 13939–13946.

19 Z. Cai, Y. Guo, S. Yang, Q. Peng, H. Luo, Z. Liu, G. Zhang, Y. Liu and D. Zhang, *Chem. Mater.*, 2013, **25**, 471–478.

20 L. E. Polander, S. P. Tiwari, L. Pandey, B. M. Seifried, Q. Zhang, S. Barlow, C. Risko, J.-L. Brédas, B. Kippelen and S. R. Marder, *Chem. Mater.*, 2011, **23**, 3408–3410.

21 G. Zhang, R. Chen, Y. Sun, B. Kang, M. Sun, H. Lu, L. Qiu, K. Cho and Y. Ding, *J. Mater. Chem. C.*, 2020, **8**, 1398–1404.

22 G. Zhang, Y. Zhao, B. Kang, S. Park, J. Ruan, H. Lu, L. Qiu, Y. Ding and K. Cho, *Chem. Mater.*, 2019, **31**, 2027–2035.